



## Highly Varied Reaction Cavities within a Single Molecular Crystal

Journal:	<i>CrystEngComm</i>
Manuscript ID	CE-ART-07-2023-000714.R1
Article Type:	Paper
Date Submitted by the Author:	22-Aug-2023
Complete List of Authors:	Ciszek, Jacob; Loyola University Chicago Carr, Michael; Loyola University Chicago Kochert, Matthew; Loyola University Chicago Waduge, Wathsala ; Illinois Wesleyan University Deye, Gregory; Loyola University Chicago Olsen, Ken; Loyola University Chicago

## Highly Varied Reaction Cavities within a Single Molecular Crystal

Michael R. Carr<sup>1</sup>, Matthew Kochert<sup>1</sup>, Wathsala L. I. Waduge<sup>2</sup>, Gregory J. Deye<sup>1</sup>,  
Kenneth W. Olsen<sup>1</sup>, and Jacob W. Ciszek<sup>\*1</sup>

<sup>1</sup>Department of Chemistry and Biochemistry, Loyola University Chicago, Chicago, Illinois, 60660, United States

<sup>2</sup>Department of Chemistry and Biochemistry, Illinois Wesleyan University, Bloomington, Illinois, 61701, United States

\* Corresponding author: E-mail address: jciszek@luc.edu (Jacob W. Ciszek)

### Abstract

Due to the challenges associated with its systematic study, the role of reaction cavities on the reactivity of molecular solids has often been built upon presumption. Incomplete understanding has thus led to numerous instances where modeling has proved ineffective. In response, this work systematically assesses five highly varied cavities of tetracene crystals which can be generated at the different facets of the crystal. The relative kinetics for the cavities were measured via energy dispersive X-ray spectroscopy for the reaction of tetracene with vapors of maleic anhydride, and effects were understood *via* molecular dynamic simulations. Steric effects on reactivity are consistent with postulated models for molecular cavities, though they require fine levels of structural detail to explain experimental trends. Stabilization effects range from confinement to repositioning of the reactant to accelerate reaction, with the latter result not dissimilar to active sites in enzymes. The measured stabilization effects highlight the need for the field of solid phase chemistry to incorporate it in models and suggest potential for a greater degree of control over reactivity in the solid phase than has been previously reported.

### Introduction

Solvent free organic reactions take the unique approach of directly reacting molecular solids through intracrystalline reaction, vapor diffusion within crystals, co-crystal reaction, or other variants thereof.<sup>1-6</sup> The advantages are innumerable, including environmentally benign synthesis, avoidance of protecting groups, reduced energy need, rate acceleration, applicability to insoluble materials, or even atomic level resolution of reactivity.<sup>7-9</sup> These reactions also intrigue chemists due to the unusual reactivity and selectivity imparted by the lack of solvent which provides access to heretofore impossible reactions.<sup>10-14</sup> All of these unique aspects are made possible by the fact that the syntheses are not bound by the many traditional rules governing organic reactivity.

Mechanistically, there has been clear and obvious study of nearly every aspect of these reactions. Initial studies focused on topochemical considerations as well as diffusion, molecular channels, and lattice energetics.<sup>15-17</sup> As the field continues to expand,<sup>3,18</sup> the last 20 years has seen significant study on molecular transport, eutectic intermediates, defect introduction, relaxation into crystalline states, or other kinetic aspects.<sup>19-23</sup> Additionally, the rise of mechanochemistry has meant numerous studies particular to this method.<sup>24</sup> Despite this continued effort, there is still one area that has proved challenging to systematically study – the reaction cavity.

The reaction cavity describes the amount of space available for reactant molecules to reposition themselves inside the crystal lattice without major distortion of the lattice.<sup>25</sup> The presence of void space surrounding the reaction site has been seen to enable significant reagent motion and dramatically impact reactivity.<sup>26,27</sup> Since first proposed in 1975,<sup>25</sup> it has remained a central tenant in reactivity<sup>28-30</sup> despite little success experimentally evaluating it. Cavity effects are challenging to study due to difficulties associated with systematically varying the packing of the crystal structure. Using a co-crystal reaction as an illustrative example, each time the cavity is to be sterically varied one must find a new polymorph of the reagent/substrate pair. Any systematic

variation thus becomes impossible. As a result, the role of a reaction cavity is generally calculated,<sup>26,27,31</sup> or inferred<sup>32–34</sup> rather than measured, despite the local environment playing a key role in modulating solid-state reactivity/selectivity.

We posit that these challenges can be circumvented by studying the kinetics of the reaction of the *surface* of a molecular crystal. In contrast to the bulk, each *facet* of a molecular crystal contains a unique environment (Fig. 1a), as dictated by the cleavage plane and the missing nearest neighbors at the surface (Fig. 1b, c). Though the topmost layer is missing at the surface, adjacent and internal molecules still generate restricted environments suitable to model cavity effects.<sup>35</sup> As such, one crystal would allow for systematic variation of exclusively the cavity parameters and could also allow us to keep the crystal identity and packing constant across a single experiment. Other complicating factors, such as diffusion, are eliminated. The degree of variation that can be examined is limited only by the number of facets which can be isolated for a given crystal which, due to the presence of non-equilibrium forms, commonly numbers in double digits.<sup>36</sup> There are technical hurdles in monitoring surface reactivity of molecular surfaces, but recent advances in the reactions of these materials<sup>23,37</sup> present the opportunity to directly observe this important parameter.

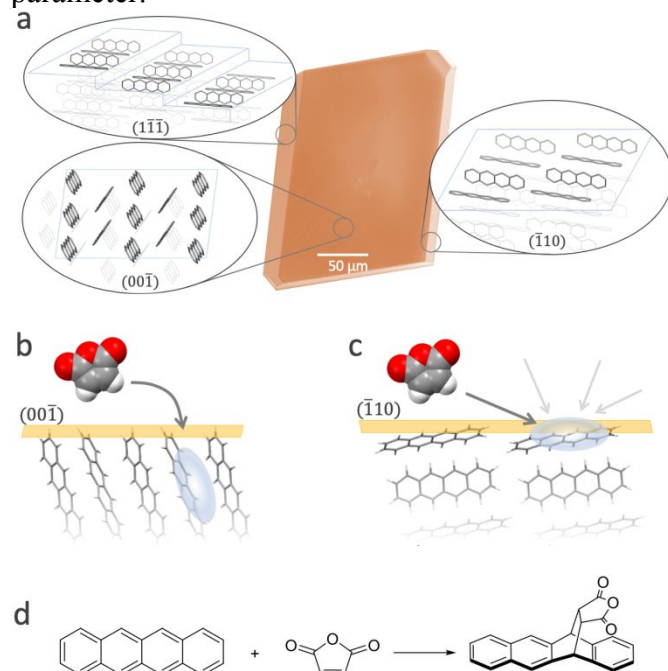


**Fig. 1.** (a) False-colored SEM image of a tetracene crystal showing structures of the (001) surface (comprising the major facet) and (110) and (111) surfaces. Crystallographic planes are highlighted with blue boxes. (b) (001) and (c) (110) surfaces of tetracene showing the approach of maleic anhydride towards the diene. The blue regions highlight the more reactive central rings where reaction occurs. Crystallographic planes are indicated in yellow. (d) The Diels-Alder reaction of tetracene with maleic anhydride, with one of the two possible diastereomer products shown.

Herein, energy dispersive X-ray spectroscopy (EDX) and computational methods were used to analyze the extent of the Diels-Alder reaction at the various facets of tetracene single crystals to systematically analyze the role reaction cavities play in solid-state reaction kinetics. Using this surface sensitive and spatially selective spectroscopy in conjunction with scanning electron microscopy (SEM) allows for the measurement and indexing of a large number of facets over hundreds of crystals, in a high throughput manner. Kinetic data is benchmarked against

molecular packing models generated from tetracene's unit cell, while molecular dynamic (MD) simulations provide detailed mechanistic clarity regarding the role of steric and stabilization components of the reaction cavity. The insights gleaned from this study significantly improve fundamental understanding of solid-state reactivity by fully examining the highly diverse role of cavities on the reactivity of solid systems.

## Results and Discussion

Briefly, the reaction between maleic anhydride and a tetracene single crystal was chosen because of significant precedence,<sup>23,37–39</sup> mechanistic simplicity,<sup>40</sup> readily assigned facets,<sup>41</sup> and ease of reaction analysis. Using a horizontal crystal growth tube, hundreds of tetracene crystals were grown on a silicon wafer with tens of them of appropriate orientation and size for analysis. As the analysis method (EDX) has an angular dependence, crystals were imaged via SEM and were selected to be vertical to assure that the electron beam generated sufficient signal (Fig. 2a). Crystals were indexed using the law of constancy of interfacial angles, and facets were confirmed by comparison to a model crystal generated via KrystalShaper (Fig. 2b, c, d). Each unique surface is identified by its three-digit miller indices from which the corresponding molecular packing at the surface can be generated (e.g., Fig. 1a-c). Using this procedure, 96 crystals were indexed, though some specific facets occurred with insufficient frequency to be analyzed (Fig. S1). A total of five surfaces were fully examined once degenerate surfaces (e.g., (001), (00 $\bar{1}$ )) were combined into a single data set.

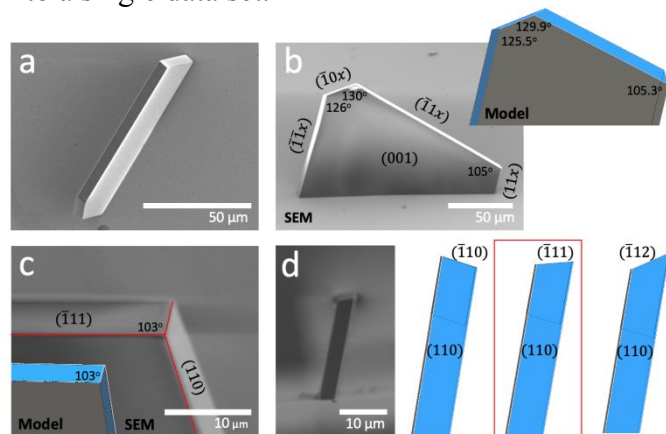


**Fig. 2.** Crystal indexing. (a) SEM image of a typical crystal vertically oriented on the surface for optimal EDX measurements. (b-c) SEM image of the crystal tilted, along with angles measured between the planes. Comparative model crystal is depicted in blue/grey color. (d) Side view SEM image of crystal showing corroboration of the final miller index.

The crystals underwent Diels-Alder reaction with vaporous maleic anhydride, whose three oxygen atoms provide elemental signal in proportion to the amount of product formed on each surface. The extent of reaction was quantified via EDX which provides the necessary sensitivity to measure down to roughly 1/3 of a surface reacted (~1% oxygen at 1 keV). As a result, differences in the C:O ratio between facets (Fig. 3) can be used to differentiate kinetics at the various surfaces. Since small amounts of beam induced damage have been known to occur,<sup>42</sup> several reference samples (a polished carbon surface and unreacted tetracene crystals) were analyzed to demonstrate negligible oxidation. Control reactions with *N*-methylmaleimide (Fig. S2) confirm the source of oxygen is from the reactant. Initial kinetics were probed at two time points (8 h and 16 h). Longer reaction times were initially performed but discontinued as the majority of surfaces showed no further increase in product.

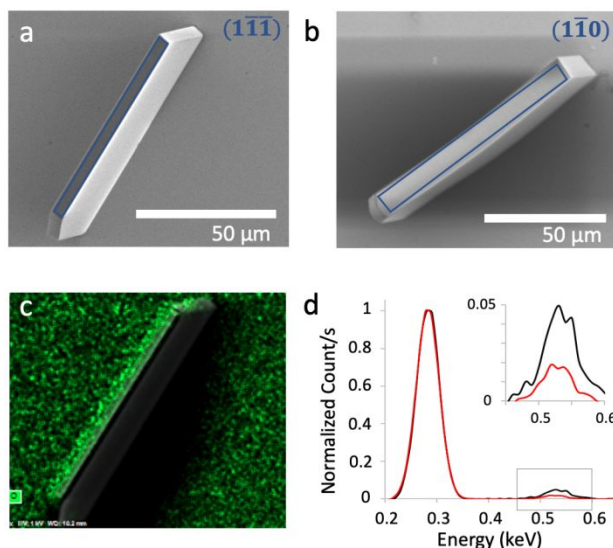


**Fig. 3.** (a, b) Example SEM images of tetracene crystals with the blue box indicating the selected region for EDX analysis. (c) EDX map of the oxygen  $K_{\alpha}$  signal (green) for the  $(1\bar{1}\bar{1})$  surface. (d) EDX spectrum for the  $(1\bar{1}0)$  and  $(1\bar{1}\bar{1})$  surfaces (red and black respectively). The prominent carbon  $K_{\alpha}$  signal at 0.277 keV has been normalized to 1. Inset shows the magnified oxygen  $K_{\alpha}$  signal at 0.525 keV.

The reactivity data is summarized in Table 1, and it is clear that the various surfaces do indeed generate distinct cavities with their own unique reactivity. But, before detailed analysis of these cavity effects, there are several data points are worth highlighting. First, the reactivity of the prominent face ( $(00\bar{1})$ ) is relatively low with the signal just exceeding the limit of detection. This is the only surface with previously reported kinetics, and the data in Table 1 is in line with those findings.<sup>37</sup> Second, many of the surfaces seem to saturate at  $\sim 3.5\text{-}4\%$  oxygen, an observation further supported by additional measurements (Fig. S1). Accordingly, reactivity analysis often centers on the time needed to reach this threshold, or on comparing points before the saturation has been reached (e.g., the  $(110)$  reacts quite fast as it has already saturated at the 8 h time point). The only exception to the 3.5-4% saturation rule was the  $(1\bar{1}\bar{1})$  surface which reaches oxygen levels markedly higher than any of the others. This was true of four samples over two trials. Though interesting, the difference in saturation is addressed in the supplementary information since it is tangential to the kinetics discussion.

**Table 1. EDX Data for Common Tetracene Crystallographic Planes after Reaction with Maleic Anhydride.**

	Surface	Oxygen percentage <sup>a</sup>	
		8 h	16 h
Sterically Distinct	$(00\bar{1})$	$1.5 \pm 0.2$	$1.7 \pm 1.1$
	$(110)$	$3.9 \pm 0.3$	$3.2 \pm 0.6$
	$(1\bar{1}0)$	$2.3 \pm 0.4$	$3.9 \pm 0.7$
	$(1\bar{1}\bar{1})$	$3.0 \pm 0.4$	$3.7 \pm 0.7$
	$(1\bar{1}\bar{1})$	$3.9 \pm 0.9$	$11.0 \pm 1.5$

<sup>a</sup> Oxygen data is weighted means and weighted standard deviations, with the weights determined by the absolute error.

To aid discussion, we have also presorted the data into two categories corresponding to the primary factors impacting the kinetics: steric hindrance of the reaction cavity and the stabilization of the reactant within the cavity. Stabilization effects refer to the cavity's ability to provide energetically preferable locations to either keep the reactant within the cavity by increasing the residence time and proximity to the site of reaction or to stabilize a particular orientation within the cavity that is similar to the transition state.<sup>43–45</sup> Steric hindrance, or inhibition of reactive sites, is so ubiquitous it requires no introduction. Due to the simplicity of the latter is analyzed first.

Of the surfaces in Table 1, the top three have been designated as being sterically distinct from each other, and the dimensions of their cavities are highlighted in Fig. 4. The (00 $\bar{1}$ ) surface contains no cavity (Fig 4a), with the tight herringbone packing placing adjacent tetracenes near van der Waal contact distance. Since the entirety of the reactive aromatic system is contained within the crystal, it is the most stable surface and its kinetics are extremely slow. The other two surfaces ((1 $\bar{1}$ 0), (110)) do have distinct cavities that are primarily a function of the molecular packing the *ab* plane (shown in the blue section in Fig. 4b). Here, the adjacent tetracenes form a channel where the maleic anhydride can reside, but which also limits access to the diene needed for the transition state shown back in Fig. 1d. This channel is ~10 Å across and can easily accommodate the maleic anhydride reactant (Fig. 4c). Moreover, since tetracene packs in a triclinic unit cell,<sup>46</sup> the angles between the *a* and *b* axes are not 90 degrees and the channel size is about 5% larger for the (1 $\bar{1}$ 0) surface compared to the (110) surface (Fig. 4d). Thus, the presumption would be that this larger cavity would have a slightly larger initial rate at 8 h than the smaller (110).

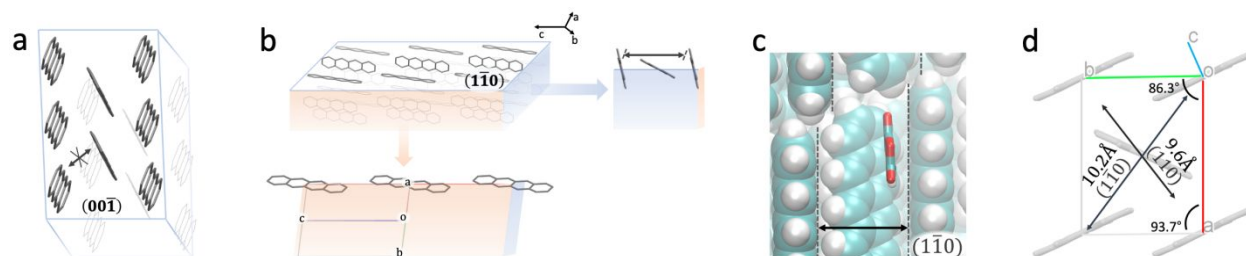


**Fig. 4.** (a) Surface structure for the sterically hindered (00 $\bar{1}$ ) surface highlighting the close packing of neighboring surface molecules. (b) Surface structure for the (1 $\bar{1}$ 0) surface (white plane), along with slices orthogonal to the plane (orange and blue) to highlight surface orientation and spacing. The double arrow in the blue slice denotes the reactive channel formed by two inaccessible vertically-oriented tetracene molecules on either side of the reactive near-planar central tetracene. (c) A space filling model of the top view of the reactive channel containing a maleic anhydride. (d) Tetracene's unit cell, highlighting the (110) and (1 $\bar{1}$ 0) cleavage planes.

When experimental kinetics were analyzed, there was some understandable surprise that the (110) and (1 $\bar{1}$ 0) surfaces ran counter to expectations. Specifically, the slightly larger channel width on the (1 $\bar{1}$ 0) surface had *notably* slower initial kinetics at the 8 hour mark compared the (110) surface. We examined three alternative explanations for this phenomenon. First, we placed the reactant in the ideal transition state for a Diels-Alder reaction<sup>47</sup> and examined the closest contact distance (Fig. 5a). This was to try and account for the fact that the hydrogens of tetracene are staggered positionally, and thus channel width might be missing this key information. Again, the result was the same with there being slightly more space for the (1 $\bar{1}$ 0) surface (1.76 vs 1.71 Å, Fig. 5a). Second, we confirmed that there were no energetic differences between the two surfaces by performing an energy minimization on maleic anhydride within the cavity. Both surfaces minimize to -12 kcal/mol (Fig. S3) ruling out any potential stabilization effects. Finally,

we reexamined the maleic anhydrides in Fig. 5a but, rather than focus on a single location with the largest closest contact, *all* available reaction sites were examined. This appears to hold the answer. It turns out that while the largest available cavity is indeed on the  $(1\bar{1}0)$  surface only half of the potential transition states are viable. For the  $(1\bar{1}0)$  surface, the configurations highlighted in red in Fig. 5b are extremely hindered with closest contacts at 1.40-1.45 Å. With two of the four approaches in the cavity unavailable the initial rate of reaction is halved, roughly mirroring what is seen the EDX measurements. In contrast, the  $(110)$  surface has similar closest contact distances across all four positions. So, this is another instance where sterics of the cavity do indeed dictate reaction, though it is based on fine cavity details rather than coarser factors such as channel size.

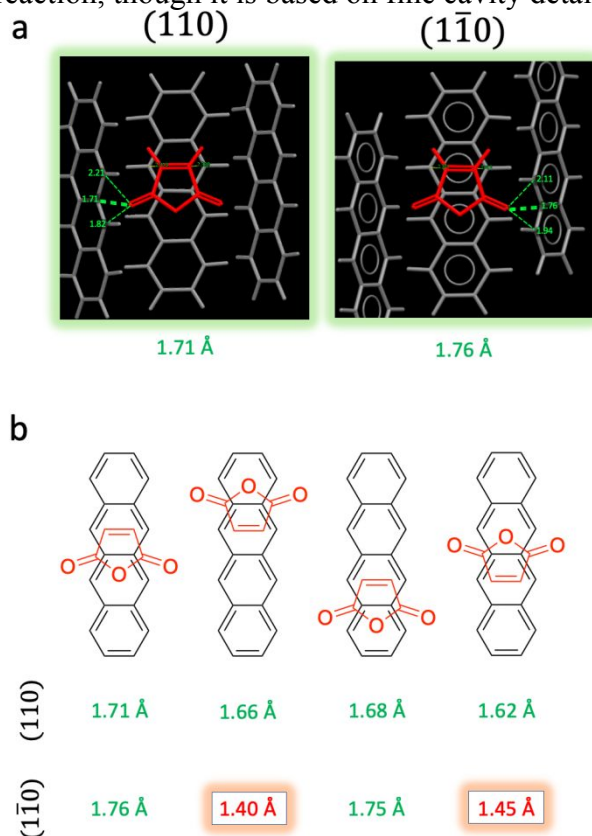


**Fig. 5.** Steric models of the closest contact of maleic anhydride placed at the optimal transition state<sup>47</sup> for Diels-Alder reaction. (a) The maleic anhydride (red) is placed 2.3 Å above the diene and the distance to the closest carbons and hydrogens are measured. Thickest dashed green line corresponds to the closest contact and the numerical distance is listed below the figure. (b) All transition states for the possible stereoisomers, with the closest contacts for the two surfaces. Full modeling data can be found in Fig. S4 and 5.

When moving to the second category of data, we examined three surfaces that are effectively identical sterically. Here stabilization effects within the cavity can be examined. This designation was given to three surfaces with miller indices of  $(1\bar{1}0)$ ,  $(1\bar{1}1)$ , and  $(1\bar{1}\bar{1})$ . These share a common interception of the a and b axis meaning the nearest neighbors are *identical*, with the c-axis difference only resulting in steps in the surface (Fig. 6a). Importantly, the neighbors in the *a-b* plane (i.e., the channel “walls”) are what block access to tetracene’s  $\pi$  system so maleic anhydride’s approach is the same for each. The trend in experimental EDX data was examined via MD simulations of maleic anhydride’s trajectories on the surface in an attempt to understand why adding steps on one end of the cavity channel significantly increases initial reaction rates. For

each simulation ten maleic anhydride molecules were allowed to move and interact at each of the tetracene surfaces, with a representative example shown in Fig. 6b, c. This allowed for the observation of adsorbed maleic anhydrides' diffusion across the surface as well as residence within the reaction cavity.

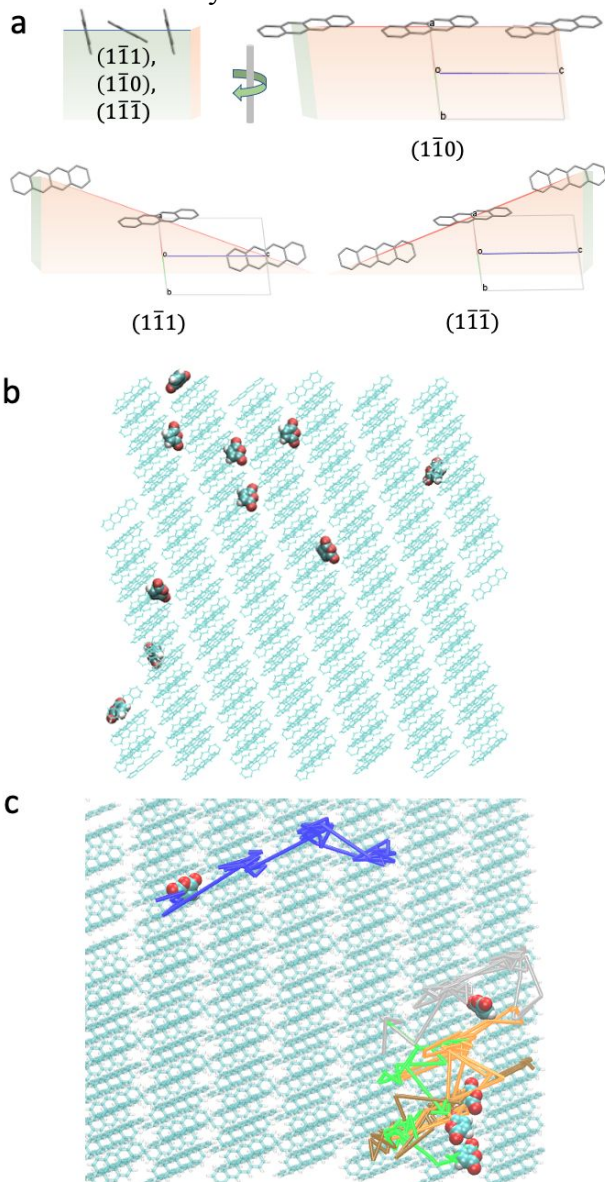


**Fig. 6.** (a) Structure for the sterically similar surfaces. In each, only the surface molecules are shown, and the orange/blue depicts the bulk portion of the crystal. Faint orange or blue line corresponds to the surface cleavage plane; labeled green, red, and blue lines are the unit cell axes, while the gray parallelogram outlines the unit cell. Image in the top left represents the common surface structure in the a-b plane. When this structure is rotated 90 degrees, the steps that differentiate the  $(1\bar{1}1)$ , and  $(1\bar{1}\bar{1})$  surfaces from the  $(1\bar{1}0)$  become apparent. (b) Final positions of the maleic anhydride molecules at the end of the MD simulation for a  $(1\bar{1}1)$  tetracene surface. (c) Path traces for five maleic anhydrides for the last half of the MD simulations on the  $(1\bar{1}0)$  surface.

These simulations (Fig. S6-10) show that the driving mechanism behind the stabilization in the cavity is much more complex and interesting than anticipated. In all three surfaces the

primary motion is within the cavity of the channel, thus the tetracenes comprising the channel's walls do stabilize and confine the reactant surface. There is also minimal variance in the interaction energies for the maleic anhydride as it traverses the length of the channel (less than 1 kcal/mol, Fig. 7a, b), so motion along the length of the cavity is facile. Once at the end of the channel, there is only a slight barrier preventing the reactant molecule from continuing along to the next tetracene. In the case of the flat  $(1\bar{1}0)$  surface, there is an average cavity residence time of 1.3 ns over a single tetracene before continuing to the next. When a step is added (Fig. 7c, d) one exit of the cavity becomes impeded. The result is that the maleic anhydride is trapped over a particular tetracene, but also that it is slightly stabilized at that end due to the interactions with the raised molecules present at the step. This stabilization was most evident in the impeded  $(1\bar{1}1)$  surface where the maleic anhydride is now -1.3 kcal/mol more stable when residing near the molecular step (Fig. 7a vs 7c). As a result, maleic anhydrides within the two stepped surfaces were generally not observed to leave the cavity once they had entered.

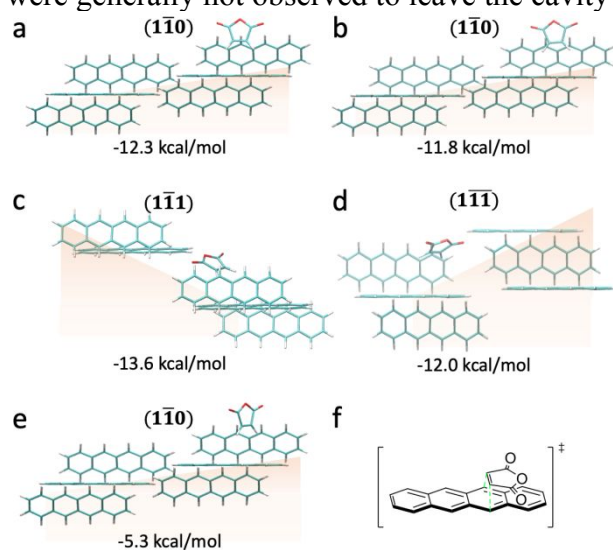


**Fig. 7.** (a-d) Energy minimized position and interaction energy of the maleic anhydride for indicated surfaces. (e) Unminimized position and interaction energy for a twisted maleic anhydride for the  $(1\bar{1}0)$  surface. (f) Lowest energy transition state for the tetracene maleic anhydride adduct.

While experiment and simulation appear to support a simplistic interpretation of kinetics, this turns out to miss an important point. Instead, the most stable *position* of the maleic anhydride plays a heavy role in the kinetics, and its ability to position near a transition state suitable for the Diels-Alder reaction has the ability to impact reactivity. The most stable position for the maleic anhydride on the  $(1\bar{1}0)$  surface is planar to the tetracenes that make the walls of the channel (Fig. 7a). This coplanar orientation is also dramatically more stable regardless of where along the length of the tetracene it is placed (e.g., Fig. 7b). Note, this is *not* a reactive tetracene based on packing arguments in Fig. S4), rather the channel walls are the least impeded and provide sufficient stabilization such that maleic anhydride should assume a coplanar orientation. As a result, the maleic anhydride is locked into a position ill-suited for reaction and also becomes significantly destabilized when twisted towards a reactive orientation (7.0 kcal/mol higher with the molecule only  $40^\circ$  off planar, Fig. 7e). In contrast, the two stepped surfaces have an additional stable configuration that is well suited for reaction (Fig. 7c, d). Here, the reactant is stabilized position where it is tilted toward the molecules of the upper step placing it in the natural pocket created by

the step edge. In addition to tilting, the reactant molecule is also allowed to twist within this pocket. This positions the maleic anhydride near its optimal transition state for the Diels-Alder reaction (Fig. 7f), with effective orbital interactions facilitating reaction within this pocket.

The specific location of the stabilizing pocket also suggests a slight difference in reaction kinetics between the  $(1\bar{1}1)$  and  $(1\bar{1}\bar{1})$  surfaces. Comparing the two stepped surfaces in Fig. 8, the reactant molecule is stabilized in a slightly different position laterally along the tetracene, as dictated by the cavity. For the  $(1\bar{1}\bar{1})$  surface the reactant is stabilized over both of the central rings of the tetracene molecule (Fig. 8a). These are the most active rings and have been shown to have relative rates five orders of magnitude faster than the exterior rings.<sup>48</sup> In contrast the  $(1\bar{1}1)$  surface stabilizes the reactant over one of the central rings and one of the exterior rings (Fig. 8b). This difference in position of the dienophile within the reactive pocket could suggest that there is a real difference between the initial reaction rate seen experimentally between the two stepped surfaces.

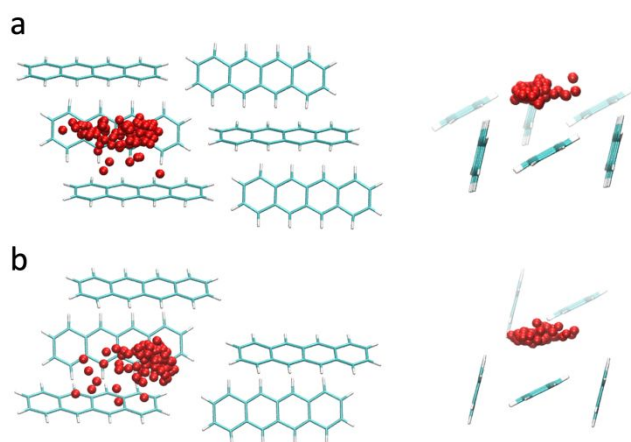


**Fig. 8.** (a,b) Heat map of maleic anhydride over a single reaction cavity on indicated surfaces. Red dots correspond to the center of mass positions for a maleic anhydride within the reaction cavity for each time point in the simulation (Left) top view. (Right) side view.

Overall, the findings on the stepped surfaces are illuminating. The ability for an organic crystal to preposition or stabilize a reactant to facilitate a reaction is not a function normally associated with reaction cavity in organic solids.<sup>49</sup> Cavities have been extensively evaluated from a steric standpoint, and the limitations of this approach are well documented.<sup>27,50,51</sup> Cavities are also known to be capable of redistributing electron density within the reactant, but here with the non-polar tetracene these effects are minimal. Rather, it is the positioning of the reagent that appears key. Perhaps the lack of mention in literature is due to the fact that mechanistically, steric factors will generally dominate reactivity – in this system sterics generated the largest variance in initial kinetics (at least a factor of 2.6 between the  $(110)$  and  $(00\bar{1})$  surfaces). So, it is only for systems where steric considerations are roughly equivalent that prepositioning of the reactant can effectively be isolated. If so, this work clearly demonstrates that these effects can be extremely important and that these considerations are potentially the missing link preventing effective modeling<sup>50–52</sup> of some solid phase reactions. Moreover, this degree of prepositioning appears not dissimilar to that seen in the active site of an enzyme, suggesting a high degree of control is possible with further improvements in modeling and cavity construction. It is possible that this

effect may eventually lead to rational control of regio- or stereoisomer formation via this mechanism.

## Conclusion

In summary, EDX spectroscopy of the various facets on hundreds of tetracene crystals provided kinetic data for the Diels-Alder reaction with maleic anhydride. This allowed for the roles of reaction cavities in solid-phase kinetics to be studied with two primary factors influencing reactivity. Steric hinderance of the reactive cavity by adjacent molecules in the crystal played the central role in reaction kinetics and significantly inhibited surfaces such as the  $(00\bar{1})$  and, to a lesser extent, the  $(1\bar{1}0)$  surface. Simple steric models based of molecular spacing were ineffective unless atomistic level details were included for all possible transition states. Stabilization considerations were clearly isolated for stepped surfaces which had identical cavity channels, but a stabilizing “cap” at the end of the channel. Kinetics were dictated by the cavity’s ability to use stabilizing interactions to orient and place the reactant in an optimal position near the natural transition state for the Diels-Alder reaction. These positioning effects were most commonly observed in the higher indexed crystallographic planes, specifically the  $(1\bar{1}1)$  and  $(1\bar{1}\bar{1})$  surfaces. This newly elucidated mechanistic understanding has broad ranging implications for understanding the unique product formation which defines reactions in the solid-phase, provides a foundation for increasing the reaction rate of known solid-phase reactions, and increases the feasibility of performing new reactions in the solid-phase.

## Author Contributions

M.R.C performed the experimental work and drafted the manuscript, M.K. performed the molecular dynamics simulations, W.L.I.W. and G.D. developed the methodology for indexing the crystals, K.O. oversaw computational studies, J.W.C. oversaw the research and wrote the final manuscript. All authors assisted in revisions and approved of the final version of the manuscript.

## Conflict of Interest

There are no conflicts to declare.

## Electronic Supplementary Information

EDX quantification of *N*-methylmaleimide reactions; average EDX data for all facets; additional projections of maleic anhydride over tetracene; additional path traces; additional energy minimization; images of all crystals.

## Acknowledgements

The authors acknowledge financial support from the National Science Foundation (NSF) under Award No. 1665433. The scanning electron microscope that was used in this study was funded by the NSF Major Research Instrumentation (MRI) award 1726994.

## References

- 1 D. Braga, L. Maini and F. Grepioni, *Chem. Soc. Rev.*, 2013, **42**, 7638–7648.
- 2 G. Cravotto, D. Garella, D. Carnaroglio, E. Calcio Gaudino and O. Rosati, *Chem. Commun.*, 2012, **48**, 11632–11634.
- 3 K. Kubota, T. Seo, K. Koide, Y. Hasegawa and H. Ito, *Nat. Commun.*, 2019, **10**, 111.
- 4 V. Štrukil and I. Sajko, *Chem. Commun.*, 2017, **53**, 9101–9104.
- 5 S. Nakamatsu, S. Toyota, W. Jones and F. Toda, *Chem. Commun.*, 2005, 3808–3810.
- 6 D. Braga, M. Cadoni, F. Grepioni, L. Maini and K. Rubini, *CrystEngComm*, 2006, **8**, 756–763.
- 7 G. W. V. Cave, C. L. Raston and J. L. Scott, *Chem. Commun.*, 2001, 2159–2169.
- 8 S. Ohba, H. Hosomi and Y. Ito, *J. Am. Chem. Soc.*, 2001, **123**, 6349–6352.
- 9 J. L. Howard, Q. Cao and D. L. Browne, *Chem. Sci.*, 2018, **9**, 3080–3094.
- 10 M. A. Sinnwell and L. R. MacGillivray, *Angew. Chem. Int. Ed.*, 2016, **55**, 3477–3480.
- 11 Z. Yang and M. A. Garcia-Garibay, *Org. Lett.*, 2000, **2**, 1963–1965.
- 12 A. M. Belenguer, T. Friščić, G. M. Day and J. K. M. Sanders, *Chem. Sci.*, 2011, **2**, 696–700.
- 13 G.-W. Wang, K. Komatsu, Y. Murata and M. Shiro, *Nature*, 1997, **387**, 583–586.
- 14 J. G. Hernández and C. Bolm, *J. Org. Chem.*, 2017, **82**, 4007–4019.
- 15 N. B. Singh, R. J. Singh and N. P. Singh, *Tetrahedron*, 1994, **50**, 6441–6493.
- 16 J. M. Thomas, *Pure Appl. Chem.*, 1979, **51**, 1065–1082.
- 17 J. M. McBride, *Acc. Chem. Res.*, 1983, **16**, 304–312.
- 18 S. Yamada, Y. Tokugawa, Y. Nojiri and E. Takamori, *Chem. Commun.*, 2012, **48**, 1763–1765.
- 19 S. L. James, C. J. Adams, C. Bolm, D. Braga, P. Collier, T. Friščić, F. Grepioni, K. D. M. Harris, G. Hyett, W. Jones, A. Krebs, J. Mack, L. Maini, A. Guy Orpen, I. P. Parkin, W. C. Shearouse, J. W. Steed and D. C. Waddell, *Chem. Soc. Rev.*, 2012, **41**, 413–447.
- 20 A. A. L. Michalchuk, I. A. Tumanov, V. A. Drebushchak and E. V. Boldyreva, *Faraday Discuss.*, 2014, **170**, 311–335.
- 21 F. Fischer, M. Joester, K. Rademann and F. Emmerling, *Chem. – Eur. J.*, 2015, **21**, 14969–14974.
- 22 K. Varga, J. Volarić and H. Vančik, *CrystEngComm*, 2015, **17**, 1434–1438.
- 23 S. Piranej, M. A. W. S. Sayers, G. J. Deye, S. N. Maximoff, J. P. Hopwood, H. Park, J. G. Slavsky and J. W. Ciszek, *CrystEngComm*, 2020, **22**, 4108–4115.
- 24 E. Boldyreva, *Chem. Soc. Rev.*, 2013, **42**, 7719–7738.
- 25 M. D. Cohen, *Angew. Chem. Int. Ed. Engl.*, 1975, **14**, 386–393.
- 26 T. Luty and C. J. Eckhardt, *J. Am. Chem. Soc.*, 1995, **117**, 2441–2452.
- 27 K. A. Konieczny, A. Szczurek, J. Bąkiewicz, R. Siedlecka, A. Ciesielski, M. K. Cyrański and I. Turowska-Tyrk, *Cryst. Growth Des.*, 2020, **20**, 5061–5071.
- 28 W. Jones, *Organic Molecular Solids: Properties and Applications*, CRC Press, Boca Raton, FL, 2019.
- 29 E. Leyva, D. de Loera, C. G. Espinosa-González and S. Noriega, *Curr. Org. Chem.*, 2019, **23**, 215–255.
- 30 Y. Ohashi, in *Crystalline State Photoreactions: Direct Observation of Reaction Processes and Metastable Intermediates*, ed. Y. Ohashi, Springer Japan, Tokyo, 2014, pp. 5–18.
- 31 A. Gavezzotti, *J. Am. Chem. Soc.*, 1983, **105**, 5220–5225.

- 32 J. N. Moorthy and K. Venkatesan, *J. Org. Chem.*, 1991, **56**, 6957–6960.
- 33 Y. Wang, X. Dong, X. Tang, H. Zheng, K. Li, X. Lin, L. Fang, G. Sun, X. Chen, L. Xie, C. L. Bull, N. P. Funnell, T. Hattori, A. Sano-Furukawa, J. Chen, D. K. Hensley, G. D. Cody, Y. Ren, H. H. Lee and H. Mao, *Angew. Chem. Int. Ed.*, 2019, **58**, 1468–1473.
- 34 Y. Ohgo, Y. Arai and S. Takeuchi, *Chem. Lett.*, 1991, **20**, 455–458.
- 35 C. Park, J. E. Park and H. C. Choi, *Acc. Chem. Res.*, 2014, **47**, 2353–2364.
- 36 D. Winn and M. F. Doherty, *AIChE J.*, 2000, **46**, 1348–1367.
- 37 B. A. Qualizza, S. Prasad, M. P. Chiarelli and J. W. Ciszek, *Chem. Commun.*, 2013, **49**, 4495.
- 38 F. Li, J. P. Hopwood, M. M. Galey, L. M. Sanchez and J. W. Ciszek, *Chem. Commun.*, 2019, **55**, 13975–13978.
- 39 B. A. Qualizza and J. W. Ciszek, *J. Phys. Org. Chem.*, 2015, **28**, 629–634.
- 40 I. Fleming, *Pericyclic Reactions*, Oxford University Press, Oxford, New York, Second Edition., 2015.
- 41 H. M. Cuppen, W. S. Graswinckel and H. Meekes, *Cryst. Growth Des.*, 2004, **4**, 1351–1357.
- 42 R. F. Egerton, P. Li and M. Malac, *Micron*, 2004, **35**, 399–409.
- 43 M. Yoshizawa, M. Tamura and M. Fujita, *Science*, 2006, **312**, 251–254.
- 44 Y. Fang, J. A. Powell, E. Li, Q. Wang, Z. Perry, A. Kirchon, X. Yang, Z. Xiao, C. Zhu, L. Zhang, F. Huang and H.-C. Zhou, *Chem. Soc. Rev.*, 2019, **48**, 4707–4730.
- 45 M. Yoshizawa, J. K. Klosterman and M. Fujita, *Angew. Chem. Int. Ed.*, 2009, **48**, 3418–3438.
- 46 J. M. Robertson, V. C. Sinclair and J. Trotter, *Acta Crystallogr.*, 1961, **14**, 697–704.
- 47 C.-X. Cui and Y.-J. Liu, *J. Phys. Org. Chem.*, 2017, **30**, e3610.
- 48 P. von R. Schleyer, M. Manoharan, H. Jiao and F. Stahl, *Org. Lett.*, 2001, **3**, 3643–3646.
- 49 E. V. Boldyreva, *Solid State Ion.*, 1997, **101–103**, 843–849.
- 50 M. A. Garcia-Garibay, *Acc. Chem. Res.*, 2003, **36**, 491–498.
- 51 K. Konieczny, J. Bąkiewicz, T. Galica, R. Siedlecka and I. Turowska-Tyrk, *CrystEngComm*, 2017, **19**, 3044–3050.
- 52 I. Halasz, *Cryst. Growth Des.*, 2010, **10**, 2817–2823.